

Optical Probing of Electronic Interaction between Graphene and Hexagonal Boron Nitride

Gwanghyun Ahn,¹ Hye Ri Kim,² Taeg Yeoung Ko,¹ Kyoungjun Choi,² Kenji Watanabe,³ Takashi Taniguchi,³ Byung Hee Hong^{2,4} and Sunmin Ryu^{1*}

¹Department of Applied Chemistry, Kyung Hee University, Yongin 446-701, Korea

²SKKU Advanced Institute of Nanotechnology (SAINT), Center for Human Interface Nano Technology (HINT) and Department of Chemistry, Sungkyunkwan University, Suwon 440-746, Korea

³National Institute for Materials Science, 1-1 Namiki, Tsukuba, 305-0044, Japan

⁴Department of Chemistry, Seoul National University, Seoul 151-747, Korea

*E-mail: sunryu@khu.ac.kr

Abstract

Even weak van der Waals (vdW) adhesion between two-dimensional solids may perturb their various materials properties owing to their low dimensionality. Although the electronic structure of graphene has been predicted to be modified by the vdW interaction with other materials, its optical characterization has not been successful. In this report, we demonstrate that Raman spectroscopy can be utilized to detect a few % decrease in the Fermi velocity (v_F) of graphene caused by the vdW interaction with underlying hexagonal boron nitride (hBN). Our study also establishes Raman spectroscopic analysis which enables separation of the effects by the vdW interaction from those by mechanical strain or extra charge carriers. The analysis reveals that spectral features of graphene on hBN are mainly affected by change in v_F and mechanical strain, but not by charge doping unlike graphene supported on SiO₂ substrates. Graphene on hBN was also found to be less susceptible to thermally induced hole doping.

Keywords: graphene, boron nitride, Raman spectroscopy, 2D band, electronic coupling

Numerous studies since the first graphene field effect transistors¹ have revealed the adverse effects of the popular SiO₂ substrates on the device performance and materials properties. In general, graphene supported on silica suffers mobility decrease due to substrate-induced ripples,²⁻⁴ scattering from charge impurities⁵⁻⁸ and surface optical phonons^{8, 9} of the substrates. The rough surface morphology of commercially available silica substrates leads to structural deformation of the supported graphene generating nanometer-scale ripples^{2, 10, 11} and charge puddles.^{7, 12} Deformed graphene is also more vulnerable to chemical attacks¹³⁻¹⁵ and develops strong p-type charge doping caused by ambient oxygen molecules.¹¹

Hexagonal boron nitride (hBN), a chemically inert and thermally robust¹⁶ dielectric material with optical bandgap of 5.97 eV,¹⁷ was the first alternative substrate to remedy the silica-induced effects providing improved carrier mobility and decreased native charge density due to its crystalline nature and lack of surface dangling bonds.¹⁸ When supported on hBN, graphene is flatter with an order-of-magnitude smaller roughness¹⁸ and slight lattice mismatch of 1.7%,¹⁹ suggesting better structural quality than that on silica substrates. Moreover, its high optical phonon frequency with dielectric properties comparable to those of silica makes hBN suitable for high temperature or electric-field applications.²⁰ Heterostructures like graphene/hBN formed by stacking 2-dimensional materials not only improve device performance but also allow new phenomena and functionalities to be discovered. Tunneling through artificial graphene bilayers sandwiching a nm-thick hBN layer obeys exponential dependence on the thickness of the spacer²¹ and the resulting field-effect tunneling transistor showed an improved on/off switching ratio of ~50.²² By controlling charge density in one graphene layer of the sandwich, Anderson localization was observed in the other graphene layer leading to metal-insulator transition.²³ Moreover, the van der Waals (vdW) interaction, despite being weak, has been predicted to lift degeneracy of the neighboring two C atoms and open up a bandgap in a Bernal-stacked graphene/hBN heterostructure,¹⁹ whereas no gap was realized in experiments^{18, 24} due to random stacking.²⁵ The vdW interlayer interaction is also manifested in stacking-dependent moire patterns in graphene/hBN,²⁶ and modulation in electronic band structures in Bernal- and random-stacked graphene bilayers.²⁷

Raman spectroscopy has been widely used in graphene study to characterize charge density,^{28, 29} mechanical strain,³⁰⁻³⁷ mix³⁸ of both, and temperature³⁹ as well as number of layers,⁴⁰ stacking⁴¹ and defects.^{40, 42} Its Raman 2D band has served as a spectroscopic fingerprint in distinguishing single-layer (1L) graphene from Bernal-stacked multilayers.⁴⁰ Random-stacking in twist graphene bilayers also

modifies the electronic structure near K points in the Brillouin zone inducing “twist angle”-dependent reduction in Fermi velocity (v_F),⁴³ non-dispersive D band,⁴⁴ and G band enhancement.^{45, 46} Unlike graphene-graphene homo-stacks, however, optical characterization of electronic coupling in hetero-stacks made of graphene and other materials has been rare despite the rising interest.⁴⁷ Because of the high sensitivity of the 2D peak frequency (ω_{2D}) to v_F , in particular, even a slight change in the electronic structure of graphene through the vdW interaction will influence the Raman spectral features, which should enable quantification of the electronic perturbation.⁴³ Understanding and separating this coupling between electronic and nuclear degrees of freedom are also important in establishing “graphene metrology” by Raman spectroscopy^{38, 48} where users have to rely on the two Raman peaks to quantify the aforementioned multiple factors.

Herein we demonstrate that the interlayer interaction modifies the linear dispersion of graphene on hBN, but not on silica, leading to $\sim 7 \text{ cm}^{-1}$ upshift in ω_{2D} , which translates into $\sim 3\%$ decrease in v_F . Unlike on silica, the native charge density of graphene is very low and annealing-induced hole doping is greatly reduced on hBN. This study shows that even weak interlayer interactions can influence Raman spectra of graphene in contact with other materials, and thus complements the Raman spectroscopic graphene metrology mainly reserved for strain^{31, 32, 48} and charge doping.^{28, 29, 38}

Results and Discussion

Hetero-stacks of graphene and hBN were prepared by a simple mechanical transfer (see Methods for details). First, thin hBN flakes were deposited on Si substrates with 285 nm-thick SiO_2 layer through mechanical exfoliation¹ of hBN crystals.¹⁷ Graphene grown on Cu foils by chemical vapor deposition method (CVD) was deposited onto the SiO_2/Si substrates with hBN flakes using the standard etching and transfer methods.⁴⁹ Figure 1a presents the optical micrograph of sample **G1**, which consists of a thin hBN layer ($\sim 20 \times 8 \text{ }\mu\text{m}^2$) and SiO_2 area both covered with graphene, denoted $1L_{\text{hBN}}$ and $1L_{\text{SiO}_2}$, respectively. Since multilayer domains ($>1 \text{ }\mu\text{m}^2$) can be easily noticed in the optical micrograph (area marked by yellow arrows in Fig. 1a & 1b), optical microscopy was used to select samples with high coverage of graphene and small ($<1\%$) areal fraction of multilayer graphene which complicates interpretation of Raman spectra.⁴³ The AFM image in Fig. 1b, obtained within the yellow box in Fig. 1a, indeed revealed that graphene covers most ($> 95\%$) of the scanned area with the rest corresponding to cracks or holes in the graphene sheet. Areas covered with multilayer graphene are scarcely found only near the torn holes

marked by the yellow arrow, indicating that the CVD growth is limited to single layer.⁴⁹ Figure 1b and 1c also show that the transfer step generated wrinkles or folds in graphene. The detailed AFM image in Fig. 1c, however, confirms that the transferred graphene is quite flat except the wrinkles suggesting good contact with the substrates. Since the graphene area corresponding to the wrinkles turned out to be less than 1% of the whole from the surface area analysis of Fig. 1c, their contribution to the Raman spectra should also be negligible (see Supporting Information, Fig. S2). The thickness of the hBN layer is 3.4 ± 0.2 nm as shown in Fig. 1d presenting the line profile averaged in the yellow rectangle in Fig. 1c. Height histograms in Fig. 1e confirm that the surface of bare hBN is much flatter than that of SiO₂ substrates:¹⁸ the standard deviation for 7 nm-thick hBN is 90 pm mostly due to instrumental noise,¹⁸ whereas that for SiO₂ is 280 pm.

Figure 2a presents two Raman spectra each obtained respectively from 1L_{SiO₂} and 1L_{BN} of Fig. 1a. The spectrum from 1L_{SiO₂} shows the two prominent Raman peaks, G and 2D respectively at ~ 1590 and ~ 2689 cm⁻¹, indicating substantial p-type charge doping as will be discussed below. The disorder-related D band also appears at ~ 1350 cm⁻¹ and the D-to-G peak height ratio (I_D/I_G) was found to be ~ 0.10 throughout the sample. Since I_D/I_G of graphene transferred onto bare SiO₂/Si substrates was ~ 0.05 , we attribute the additional D intensity to the wrinkles, cracks and holes aggravated during the transfer of graphene by the presence of hBN flakes and adhesive residues on hBN/SiO₂/Si. To further confirm the thickness of the CVD-grown graphene, we quantified the amount of C atoms using the G peak area (A_G) of mechanically exfoliated graphene which follows a quasi-linear relation between its A_G and thickness⁵⁰ (Supporting Information, Fig. S1). A_G of the CVD-grown 1L graphene turned out to lie within 10% from that of exfoliated 1L graphene, corroborating the thickness assignment. However, A_G of CVD-grown random-stacked 2L graphene in Fig. S1 was equal to or significantly larger than that of exfoliated 2L graphene. The enhancement in A_G , due to the singularities in the joint density of states,⁴⁵ limits reliable thickness characterization in random-stacked multilayers. It is to be noted that the intensity, lineshape and linewidth (Γ_{2D}) of 2D also vary nonlinearly as a function of the twist angle in random-stacked bilayers^{45,46} and that Γ_{2D} and A_{2D}/A_G are much less useful in determining thickness than A_G (Fig. S1).

The spectrum of 1L_{BN} in Fig. 2a shows another sharp peak at 1366 cm⁻¹, originating from the E_{2g} phonon mode of hBN crystal.⁵¹ The spectral details of the hBN peak were obtained by separation from the D peak through a curve fitting as shown in Fig. 2a. The Raman map for the hBN peak area (A_{BN}) in Fig. 2b matches well with the optical micrograph and AFM images in Fig. 1. Whereas the G and 2D peaks are also most prominent in 1L_{BN}, their spectral details are distinct from those of 1L_{SiO₂}. The G peak frequency ($\omega_G \sim 1584$ cm⁻¹), ~ 6 cm⁻¹ lower than that from 1L_{SiO₂}, is more closer to the intrinsic value of graphene

$(\omega_G^0 \sim 1581.5 \text{ cm}^{-1})$,³⁸ which can also be seen in the ω_G -map in Fig. 2c. Additionally, the spectra reveal the linewidth of the G peak (Γ_G) and 2D-to-G peak area ratio (A_{2D}/A_G) are larger for $1L_{BN}$ than $1L_{SiO_2}$. These spectral differences, occurring throughout the sample as shown in the Raman maps of Fig. 2e & 2f, can be explained by reduced charge doping¹⁸ in $1L_{BN}$ as will be discussed below and are consistent with the scanning tunneling microscopy study of CVD graphene on hBN.²⁶ However, we note that the change in ω_{2D} from its intrinsic value ($\omega_{2D}^0 \sim 2677 \text{ cm}^{-1}$)³⁸ is unusually high ($\Delta\omega_{2D} \sim 11 \text{ cm}^{-1}$) and cannot be solely attributed to mechanical strain or charge doping, since $\Delta\omega_G$ is only $\sim 2.5 \text{ cm}^{-1}$ and thus $\Delta\omega_{2D}/\Delta\omega_G$ is larger than 4.³⁸

To interpret the anomalous behavior of ω_{2D} , we employed the analysis recently proposed by J. Lee *et al.*,³⁸ which distinguishes the effects of the two most influential factors in Raman spectra of graphene, mechanical strain³⁰⁻³⁷ and charge doping.^{28, 29} The Raman peak frequencies (ω_G, ω_{2D}) of graphene under tensile (compressive) stress will move from the intrinsic value of strain-free and charge-neutral graphene, $\mathbf{O}(\omega_G^0, \omega_{2D}^0)$,³⁸ along the \mathbf{e}_T (\mathbf{e}_C) vector representing tensile (compressive) strain as shown in the inset of Fig. 3a. Hole doping will move (ω_G, ω_{2D}) along the \mathbf{e}_H vector in the inset as the data from an electrical gating measurement⁵² show in Fig. 3a (red solid line). Using strain (ϵ) and charge density (n) values marked on the \mathbf{e}_T and \mathbf{e}_H axes, any given (ω_G, ω_{2D}) can then be vector-decomposed into ϵ and n .³⁸ For instance, two groups of (ω_G, ω_{2D}) points³⁸ obtained from a graphene sample mechanically exfoliated from graphite (Fig. 3a) clearly reveal its pristine state with varying native strain ($-0.1\% < \epsilon < 0.4\%$) but negligible charge density (brown squares) and hole-doped state ($n \sim 1.4 \times 10^{13} \text{ cm}^{-2}$) induced by thermal annealing (brown triangles).

When projected onto the (ω_G, ω_{2D}) space in Fig. 3a, the Raman data of two samples **G1** and **G2** processed in the same conditions with similar hBN thickness are grouped into two distinct regions, each for $1L_{SiO_2}$ (circles) and $1L_{BN}$ (crosses), respectively. All the samples studied showed the same grouping behavior (see Supporting Information). As previously mentioned regarding Fig. 2, Fig. 3 clearly shows that $1L_{SiO_2}$ areas suffer hole doping of varying density ($n < 4 \times 10^{12} \text{ cm}^{-2}$) with **G2** less doped than **G1**. Figure 3 further reveals that the spread in (ω_G, ω_{2D}) due to strain in $1L_{SiO_2}$ areas is much smaller than that due to varying charge density. Now we note that $1L_{BN}$ shows a very different spectral behavior. The data points for $1L_{BN}$ are centered around $(1583.3, 2687.9) \text{ cm}^{-1}$ for **G1** and $(1583.9, 2688.5) \text{ cm}^{-1}$ for **G2** in the forbidden zone³⁸ which cannot be reached by a linear combination of strain (\mathbf{e}_T or \mathbf{e}_C) and hole doping (\mathbf{e}_H). We attribute this anomaly in $1L_{BN}$ to modification of graphene's electronic structure caused by vdW interaction with hBN. More specifically, modulation in the dispersion of π or π^* bands, approximated as change in v_F ,²⁷ leads to change in observed ω_{2D} , since D phonon mode of different wave vector will be

selected by the double resonance processes.⁴³ Since ω_G originating from the E_{2g} zone center phonon should not be affected to a first-order approximation, the electronic modulation causing reduction in v_F should move (ω_G, ω_{2D}) along \mathbf{e}_{FVR} (denoting Fermi velocity reduction) as shown in the inset of Fig. 3a.

However, a given (ω_G, ω_{2D}) cannot be decomposed along the three unit vectors unambiguously, since all three vectors in 2-dimension cannot be independent of each other. Thus separation of the contributions from the three factors requires knowledge of at least one of the three. In Fig. 3b, we present A_{2D}/A_G which decreases rapidly as increasing $|n|$.⁵³ It can be seen that the ratios for $1L_{BN}$ (5.6 ± 0.2 for **G1**; 6.0 ± 0.2 for **G2**) are large and close to those for charge-neutral graphene denoted by the green dot (6.2 ± 0.2) in Fig. 3b while that for $1L_{SiO_2}$ is significantly smaller and widely spread just like ω_G in Fig. 3a. Since A_{2D}/A_G is very sensitive to low level of charge density,⁵³ we conclude that n of $1L_{BN}$ areas is very small and insignificant compared to $n \sim 2 \times 10^{12} \text{ cm}^{-2}$ for **G2**'s $1L_{SiO_2}$. Assuming that the spectral changes for $1L_{BN}$ occurred only along $-\mathbf{e}_T$ (\mathbf{e}_C) or \mathbf{e}_{FVR} , the change in ω_{2D} along \mathbf{e}_{FVR} ($\Delta\omega_{2D}^{FVR}$) can be estimated to be 7.2 and 6.5 cm^{-1} for **G1** and **G2**, respectively. The analysis also leads to the fact that both $1L_{BN}$ areas are slightly compressed with $\epsilon \sim -0.1\%$. The estimated degree of strain, however, is subject to whether the strain is uniaxial or biaxial.³⁸ Whereas graphene grown on Cu foils through CVD is likely to be under biaxial stress due to isotropic differential thermal expansion of Cu,^{54, 55} it was shown that the substrate-induced strain (or charge doping) is largely removed when transferred onto other substrates.⁵⁶ In addition, graphene may undergo further mechanical deformation during wet etching and transfer processes using polymer supports.⁴⁹ Although the nature of the native strain in **G1** and **G2** samples cannot be further revealed, it is to be noted that graphene mechanically exfoliated onto silica substrates is mostly under randomly oriented uniaxial stress,³⁸ implying that random mechanical perturbation like mechanical exfoliation or physical transfer favors uniaxial stress unlike the isotropic thermal perturbation.

In Fig. 4a, we investigated $1L_{BN}$ regarding spectral changes due to thermal stress which causes O_2 -induced hole doping and compression in mechanically exfoliated graphene on SiO_2 substrates as shown in Fig. 3a by brown symbols.^{11, 38} Upon thermal annealing at $400 \text{ }^\circ\text{C}$ for 2 hours, $1L_{SiO_2}$ of sample **G3** showed a drastic change in (ω_G, ω_{2D}) , which corresponds to $\Delta n \sim 1 \times 10^{13} \text{ cm}^{-2}$ confirming emergence of the strong hole doping.³⁸ In contrast, the spectral change of $1L_{BN}$ was much less and associated Δn is only $\sim 3 \times 10^{12} \text{ cm}^{-2}$. A_{2D}/A_G ratios in Fig. 4b also confirm that $1L_{BN}$ is much less susceptible to the thermal perturbation. The distribution of peak frequencies and area ratios increased by annealing can be attributed to the spectral inhomogeneity caused by structural deformation or *in-situ* reactions at elevated temperature.³⁸

Our study shows that hBN induces much less charge doping in graphene upon thermal annealing than SiO₂ substrates. Whereas exact mechanistic understanding has yet to be made, the thermally induced hole doping in graphene on SiO₂ is caused by ambient oxygen molecules in the presence of water molecules.^{11, 13} The molecular doping is also apparently connected to thermal generation¹¹ of microscopic ripples caused by conformal adhesion⁵⁷ to rough substrates or slipping-rippling³⁸ due to negative thermal expansion of graphene. Since hBN is highly flat and also has negative thermal expansion coefficient⁵⁸ unlike SiO₂, thermal rippling is expected to be much less on hBN. Moreover, hydrophobic hBN surface should contain or attract less water which enhances the O₂-induced hole doping than hydrophilic SiO₂ abundant with surface silanol groups.⁵⁹ Since the charge doping is activated by thermal treatment at as low as 100°C,³⁸ alternative substrates like hBN will be useful in future graphene applications which require reliable control of charge density or electrical conductivity.

The current study also reveals noticeable effects of hBN on the Raman spectra of graphene. Because of the random relative orientations and translations,²⁷ however, the interlayer interaction in our 1L_{BN} samples is expected to be smaller than that for graphene in good stacking registry with hBN like AA' and AB, for which theory predicted adhesion energy of 20 ~ 30 meV/C atom.¹⁹ It is also to be noted that the adhesion energy is significantly lower than the interlayer cohesive energy in graphite (61 meV/C atom)⁶⁰ or adhesion energy between graphene and SiO₂ substrates (74 meV/C atom).⁶¹ Despite the weak vdW interaction, however, the observed $\Delta\omega_{2D}^{FVR}$ for 1L_{BN} is significant enough to estimate the degree of modification in the electronic structure. Theory predicted that interlayer coupling in twist bilayer graphene preserves the linear dispersion near K points but with reduced v_F which is dependent on the twist angle.²⁷ Using Raman spectroscopy, Ni *et al.* determined $\Delta v_F/v_F$, reduction in v_F of twist bilayer graphene, which varied from -2 to -6% for several samples with unknown twist angles.⁴³ Similarly, one can estimate the change in 1L_{BN} using $\Delta v_F/v_F = 0.00449 \Delta\omega_{2D}^{FVR}$ which has been modified from what Ni *et al.* derived considering different ω_{2D}^0 and excitation photon energy: The values of $\Delta\omega_{2D}^{FVR}$ for 1L_{BN} lead to $\Delta v_F/v_F$ of -3.2 and -2.9% for **G1** and **G2**, respectively.

Now we discuss the effects of vdW interaction with SiO₂ substrates on the two Raman modes. Despite many Raman spectroscopy studies on graphene supported on SiO₂/Si substrates, the effects of vdW interaction on v_F and phonon frequency have not been clearly understood because of the overwhelmingly large spectral variations caused by native charges and strain.^{38, 62} Recently, however, J. Lee *et al.* showed that (ω_G, ω_{2D}) of charge-neutral graphene supported on SiO₂ nicely follows the e_T line, which indicates that the spectral variation is exclusively due to native strain.³⁸ Despite the significant interfacial adhesion,⁶¹ their data show no apparent movement along e_{FVR} within their experimental uncertainty of 1

cm^{-1} , implying negligible change in v_F and thus ω_{2D} . This may be attributed to the fact that SiO_2 is in amorphous phase thus not providing periodic perturbation to the band structure. Furthermore, the partial suspension on SiO_2 substrates^{38, 63, 64} may reduce the effects of the underlying substrates. On the other hand, the vdW interaction may change the force constants of the Raman modes directly. Direct observation of the change, however, is not straightforward due to the large native spectral variations in graphene supported on SiO_2 substrates. Viewing the fact that ω_G of freestanding graphene^{38, 65} is almost identical to that of Bernal-stacked graphite which is essentially vdW-type complex of graphene, one may predict that ω_G is not strongly affected by vdW interaction with SiO_2 substrates which have similar interaction energy as the interlayer cohesion energy in graphite. J. Lee *et al.*'s data also suggest that ω_G is not directly affected by the vdW interaction with SiO_2 substrates.³⁸ We also note the Raman spectroscopy work⁶⁶ by C. Lee *et al.* on single layer of semiconducting MoS_2 , where the frequencies of E_{2g}^1 and A_{1g} Raman modes were found to be highly homogeneous unlike graphene. Exploiting freestanding MoS_2 , they showed that the frequencies of the two Raman modes are not affected (within 0.3 cm^{-1}) by the presence of SiO_2 substrates.

Although there have been many Raman spectroscopy studies on graphene with mechanical strain and extra charge carriers both mediated by underlying substrates and environment, systematic and quantitative analysis has not been performed to separate the effects of both until J. Lee *et al.*'s report.³⁸ For example, random stiffening of G and 2D modes observed in pristine graphene on amorphous⁶² or crystalline insulators⁶⁷ was attributed to spontaneous p or n-type doping without considering native strain. The spectral changes in graphene that underwent thermal treatments were controversially interpreted as either mechanical compression^{68, 69} or chemical charge doping.^{11, 13, 70, 71} Some chemical treatments were considered to result in charge doping exclusively.^{14, 72} Epitaxial graphene grown on 6H-SiC^{56, 73-75} and Ru(0001)⁷⁶ has been claimed dominated by strain with minor charge doping. All of these systems are potentially susceptible to multiple perturbations simultaneously. In this regard, our work should provide a further refined approach in graphene metrology using Raman spectroscopy complementing the recent work³⁸ by J. Lee *et al.* In particular, graphene on crystalline substrates, like graphene on hBN, may be also affected by the interfacial vdW interaction in addition to strain or charge transfer, which demands careful interpretation as proposed in the current study. Despite its utility, however, our approach cannot avoid the inherent limitation that mix of more than two factors cannot be disentangled in ω_G - ω_{2D} space without additional information. Furthermore, the effect of n-type charge doping on $\Delta\omega_{2D}/\Delta\omega_G$ is highly nonlinear unlike that of p-type,³⁸ which would complicate its separation.

Conclusion

In summary, we have demonstrated that weak vdW interaction between graphene and crystalline substrates can be detected by Raman spectroscopy. Whereas ω_G is not affected, ω_{2D} increases due to the decrease in the Fermi velocity of graphene caused by the adhesion on hBN. This observation establishes a simple optical method to separate the effects of the vdW interaction entangled with those of mechanical strain or charge doping. The current study also reveals that Raman spectra of graphene on hBN are mostly affected by the vdW interaction and mechanical strain, but negligibly by charge doping, which contrasts with graphene supported on SiO₂ substrates. The proposed analysis should serve as a fast and reliable optical probe of strain or excess charges in graphene suffering vdW interaction with underlying crystalline substrates.

Methods

Preparation of graphene/hBN samples. Using mechanical exfoliation¹ of hBN crystals,¹⁷ thin hBN flakes were first deposited on Si substrates which were covered with 285 nm-thick SiO₂ layer. Then, graphene grown on Cu foils by the CVD method was deposited onto the SiO₂/Si substrates decorated with the thin hBN flakes using the standard etching and transfer methods.⁴⁹ The thickness of hBN flakes and morphology of the hetero-stacks were revealed by atomic force microscopy (AFM; XE-70, Park Systems). To avoid complication due to possible mechanical strain in graphene enveloping hBN flakes, flakes thinner than 7 nm were chosen for this study. Thermal annealing was carried out for 2 hours at specified temperature in a vacuum tube furnace maintained below 3 mTorr.

Raman spectroscopy. The Raman spectra were obtained by a home-built micro-Raman setup also detailed previously.³⁸ Briefly, excitation laser beam with a power of 1.5 mW operated at 514.5 nm was focused onto a spot of 0.5 μm in diameter using a 40 times objective lens with a numerical aperture of 0.6, which then collected backscattered Raman signal. Spectral accuracy was better than 1.0 cm^{-1} as described in a recent report.³⁸ To obtain statistically meaningful data, Raman mapping was carried out in a region of $>20 \times 20 \mu\text{m}^2$ per each sample by raster-scanning every 1 μm along x and y axes, thus providing more than 400 independent probe spots.

Acknowledgments

This work was supported by the National Research Foundation of Korea (No. 2012-053500, 2012-043136, 2012-0003059, 2011-0021972).

Supporting information available

Optical determination of thickness using A_G , surface area of wrinkles, Raman spectral analysis of additional graphene-BN samples. This material is available free of charge *via* the Internet at <http://pubs.acs.org>.

References

1. Novoselov, K. S.; Geim, A. K.; Morozov, S. V.; Jiang, D.; Zhang, Y.; Dubonos, S. V.; Grigorieva, I. V.; Firsov, A. A. Electric Field Effect in Atomically Thin Carbon Films. *Science* 2004, 306, 666-9.
2. Ishigami, M.; Chen, J. H.; Cullen, W. G.; Fuhrer, M. S.; Williams, E. D. Atomic Structure of Graphene on SiO₂. *Nano Lett.* 2007, 7, 1643-1648.
3. Katsnelson, M. I.; Geim, A. K. Electron Scattering on Microscopic Corrugations in Graphene. *Philos. Trans. R. Soc. A-Math. Phys. Eng. Sci.* 2008, 366, 195-204.
4. Morozov, S. V.; Novoselov, K. S.; Katsnelson, M. I.; Schedin, F.; Elias, D. C.; Jaszczak, J. A.; Geim, A. K. Giant Intrinsic Carrier Mobilities in Graphene and Its Bilayer. *Phys. Rev. Lett.* 2008, 100, 016602.
5. Ando, T. Screening Effect and Impurity Scattering in Monolayer Graphene. *J. Phys. Soc. Jpn.* 2006, 75, 074716.
6. Nomura, K.; MacDonald, A. H. Quantum Transport of Massless Dirac Fermions. *Phys. Rev. Lett.* 2007, 98, 076602.
7. Hwang, E. H.; Adam, S.; Das Sarma, S. Carrier Transport in Two-Dimensional Graphene Layers. *Phys. Rev. Lett.* 2007, 98, 186806.
8. Chen, J. H.; Jang, C.; Xiao, S. D.; Ishigami, M.; Fuhrer, M. S. Intrinsic and Extrinsic Performance Limits of Graphene Devices on SiO₂. *Nat. Nanotechnol.* 2008, 3, 206-209.
9. Fratini, S.; Guinea, F. Substrate-Limited Electron Dynamics in Graphene. *Phys. Rev. B* 2008, 77, 195415.
10. Stolyarova, E.; Rim, K. T.; Ryu, S.; Maultzsch, J.; Kim, P.; Brus, L. E.; Heinz, T. F.; Hybertsen, M. S.; Flynn, G. W. High-Resolution Scanning Tunneling Microscopy Imaging of Mesoscopic Graphene Sheets on an Insulating Surface. *Proc. Natl. Acad. Sci. U.S.A.* 2007, 104, 9209-9212.
11. Ryu, S.; Liu, L.; Berciaud, S.; Yu, Y.-J.; Liu, H.; Kim, P.; Flynn, G. W.; Brus, L. E. Atmospheric Oxygen Binding and Hole Doping in Deformed Graphene on a SiO₂ Substrate. *Nano Lett.* 2010, 10, 4944-4951.
12. Martin, J.; Akerman, N.; Ulbricht, G.; Lohmann, T.; Smet, J. H.; Von Klitzing, K.; Yacoby, A. Observation of Electron-Hole Puddles in Graphene Using a Scanning Single-Electron Transistor. *Nat. Phys.* 2008, 4, 144-148.

13. Liu, L.; Ryu, S.; Tomasik, M. R.; Stolyarova, E.; Jung, N.; Hybertsen, M. S.; Steigerwald, M. L.; Brus, L. E.; Flynn, G. W. Graphene Oxidation: Thickness Dependent Etching and Strong Chemical Doping. *Nano Lett.* 2008, 8, 1965-1970.
14. Liu, H.; Ryu, S.; Chen, Z.; Steigerwald, M. L.; Nuckolls, C.; Brus, L. E. Photochemical Reactivity of Graphene. *J. Am. Chem. Soc.* 2009, 131, 17099–17101.
15. Ryu, S.; Han, M. Y.; Maultzsch, J.; Heinz, T. F.; Kim, P.; Steigerwald, M. L.; Brus, L. E. Reversible Basal Plane Hydrogenation of Graphene. *Nano Lett.* 2008, 8, 4597-4602.
16. Cofer, C. G.; Economy, J. Oxidative and Hydrolytic Stability of Boron-Nitride - a New Approach to Improving the Oxidation Resistance of Carbonaceous Structures. *Carbon* 1995, 33, 389-395.
17. Watanabe, K.; Taniguchi, T.; Kanda, H. Direct-Bandgap Properties and Evidence for Ultraviolet Lasing of Hexagonal Boron Nitride Single Crystal. *Nat. Mater.* 2004, 3, 404-409.
18. Dean, C. R.; Young, A. F.; Meric, I.; Lee, C.; Wang, L.; Sorgenfrei, S.; Watanabe, K.; Taniguchi, T.; Kim, P.; Shepard, K. L.; *et al.* Boron Nitride Substrates for High-Quality Graphene Electronics. *Nat. Nanotechnol.* 2010, 5, 722-726.
19. Giovannetti, G.; Khomyakov, P. A.; Brocks, G.; Kelly, P. J.; van den Brink, J. Substrate-Induced Band Gap in Graphene on Hexagonal Boron Nitride: Ab Initio Density Functional Calculations. *Phys. Rev. B* 2007, 76, 073103.
20. Meric, I.; Han, M. Y.; Young, A. F.; Ozyilmaz, B.; Kim, P.; Shepard, K. L. Current Saturation in Zero-Bandgap, Topgated Graphene Field-Effect Transistors. *Nat. Nanotechnol.* 2008, 3, 654-659.
21. Britnell, L.; Gorbachev, R. V.; Jalil, R.; Belle, B. D.; Schedin, F.; Katsnelson, M. I.; Eaves, L.; Morozov, S. V.; Mayorov, A. S.; Peres, N. M. R.; *et al.* Electron Tunneling through Ultrathin Boron Nitride Crystalline Barriers. *Nano Lett.* 2012, 12, 1707-1710.
22. Britnell, L.; Gorbachev, R. V.; Jalil, R.; Belle, B. D.; Schedin, F.; Mishchenko, A.; Georgiou, T.; Katsnelson, M. I.; Eaves, L.; Morozov, S. V.; *et al.* Field-Effect Tunneling Transistor Based on Vertical Graphene Heterostructures. *Science* 2012, 335, 947-950.
23. Ponomarenko, L. A.; Geim, A. K.; Zhukov, A. A.; Jalil, R.; Morozov, S. V.; Novoselov, K. S.; Grigorieva, I. V.; Hill, E. H.; Cheianov, V. V.; Fal'ko, V. I.; *et al.* Tunable Metal-Insulator Transition in Double-Layer Graphene Heterostructures. *Nat. Phys.* 2011, 7, 958-961.
24. Xue, J. M.; Sanchez-Yamagishi, J.; Bulmash, D.; Jacquod, P.; Deshpande, A.; Watanabe, K.; Taniguchi, T.; Jarillo-Herrero, P.; Leroy, B. J. Scanning Tunneling Microscopy and Spectroscopy of Ultra-Flat Graphene on Hexagonal Boron Nitride. *Nat. Mater.* 2011, 10, 282-285.
25. Kharche, N.; Nayak, S. K. Quasiparticle Band Gap Engineering of Graphene and Graphone on Hexagonal Boron Nitride Substrate. *Nano Lett.* 2011, 11, 5274-5278.
26. Decker, R.; Wang, Y.; Brar, V. W.; Regan, W.; Tsai, H. Z.; Wu, Q.; Gannett, W.; Zettl, A.; Crommie, M. F. Local Electronic Properties of Graphene on a BN Substrate *via* Scanning Tunneling Microscopy. *Nano Lett.* 2011, 11, 2291-2295.
27. dos Santos, J.; Peres, N. M. R.; Castro, A. H. Graphene Bilayer with a Twist: Electronic Structure. *Phys. Rev. Lett.* 2007, 99, 256802.
28. Yan, J.; Zhang, Y.; Kim, P.; Pinczuk, A. Electric Field Effect Tuning of Electron-Phonon Coupling in Graphene. *Phys. Rev. Lett.* 2007, 98, 166802/1-166802/4.
29. Pisana, S.; Lazzeri, M.; Casiraghi, C.; Novoselov, K. S.; Geim, A. K.; Ferrari, A. C.; Mauri, F. Breakdown of the Adiabatic Born-Oppenheimer Approximation in Graphene. *Nat. Mater.* 2007, 6, 198-201.
30. Ni, Z. H.; Yu, T.; Lu, Y. H.; Wang, Y. Y.; Feng, Y. P.; Shen, Z. X. Uniaxial Strain on Graphene: Raman Spectroscopy Study and Band-Gap Opening. *ACS Nano* 2008, 2, 2301-2305.
31. Mohiuddin, T. M. G.; Lombardo, A.; Nair, R. R.; Bonetti, A.; Savini, G.; Jalil, R.; Bonini, N.; Basko, D. M.; Galiotis, C.; Marzari, N.; *et al.* Uniaxial Strain in Graphene by Raman

- Spectroscopy: G Peak Splitting, Grüneisen Parameters, and Sample Orientation. *Phys. Rev. B* 2009, 79, 205433.
32. Huang, M.; Yan, H.; Chen, C.; Song, D.; Heinz, T. F.; Hone, J. Phonon Softening and Crystallographic Orientation of Strained Graphene Studied by Raman Spectroscopy. *Proc. Natl. Acad. Sci. USA* 2009, 106, 7304-7308.
 33. Tsoukleri, G.; Parthenios, J.; Papagelis, K.; Jalil, R.; Ferrari, A. C.; Geim, A. K.; Novoselov, K. S.; Galiotis, C. Subjecting a Graphene Monolayer to Tension and Compression. *Small* 2009, 5, 2397-2402.
 34. Ding, F.; Ji, H. X.; Chen, Y. H.; Herklotz, A.; Dorr, K.; Mei, Y. F.; Rastelli, A.; Schmidt, O. G. Stretchable Graphene: A Close Look at Fundamental Parameters through Biaxial Straining. *Nano Lett.* 2010, 10, 3453-3458.
 35. Metzger, C.; Re mi, S.; Liu, M.; Kusminskiy, S. V.; Neto, A. H. C.; Swan, A. K.; Goldberg, B. B. Biaxial Strain in Graphene Adhered to Shallow Depressions. *Nano Lett.* 2010, 10, 6-10.
 36. Yoon, D.; Son, Y. W.; Cheong, H. Strain-Dependent Splitting of the Double-Resonance Raman Scattering Band in Graphene. *Phys. Rev. Lett.* 2011, 106, 155502.
 37. Zabel, J.; Nair, R. R.; Ott, A.; Georgiou, T.; Geim, A. K.; Noyoselov, K. S.; Casiraghi, C. Raman Spectroscopy of Graphene and Bilayer under Biaxial Strain: Bubbles and Balloons. *Nano Lett.* 2012, 12, 617-621.
 38. Lee, J. E.; Ahn, G.; Shim, J.; Lee, Y. S.; Ryu, S. Optical Separation of Mechanical Strain from Charge Doping in Graphene. *Nat. Commun.* 2012, 3, 1024.
 39. Calizo, I.; Balandin, A. A.; Bao, W.; Miao, F.; Lau, C. N. Temperature Dependence of the Raman Spectra of Graphene and Graphene Multilayers. *Nano Lett.* 2007, 7, 2645.
 40. Ferrari, A. C.; Meyer, J. C.; Scardaci, V.; Casiraghi, C.; Lazzeri, M.; Mauri, F.; Piscanec, S.; Jiang, D.; Novoselov, K. S.; Roth, S.; *et al.* Raman Spectrum of Graphene and Graphene Layers. *Phys. Rev. Lett.* 2006, 97, 187401/1-187401/4.
 41. Lui, C. H.; Li, Z. Q.; Chen, Z. Y.; Klimov, P. V.; Brus, L. E.; Heinz, T. F. Imaging Stacking Order in Few-Layer Graphene. *Nano Lett.* 2011, 11, 164-169.
 42. Lucchese, M. M.; Stavale, F.; Ferreira, E. H. M.; Vilani, C.; Moutinho, M. V. O.; Capaz, R. B.; Achete, C. A.; Jorio, A. Quantifying Ion-Induced Defects and Raman Relaxation Length in Graphene. *Carbon* 2010, 48, 1592-1597.
 43. Ni, Z. H.; Wang, Y. Y.; Yu, T.; You, Y. M.; Shen, Z. X. Reduction of Fermi Velocity in Folded Graphene Observed by Resonance Raman Spectroscopy. *Phys. Rev. B* 2008, 77, 235403.
 44. Gupta, A. K.; Tang, Y. J.; Crespi, V. H.; Eklund, P. C. Nondispersive Raman D Band Activated by Well-Ordered Interlayer Interactions in Rotationally Stacked Bilayer Graphene. *Phys. Rev. B* 2010, 82, 241406.
 45. Havener, R. W.; Zhuang, H. L.; Brown, L.; Hennig, R. G.; Park, J. Angle-Resolved Raman Imaging of Inter Layer Rotations and Interactions in Twisted Bilayer Graphene. *Nano Lett.* 2012, 12, 3162-3167.
 46. Kim, K.; Coh, S.; Tan, L. Z.; Regan, W.; Yuk, J. M.; Chatterjee, E.; Crommie, M. F.; Cohen, M. L.; Louie, S. G.; Zettl, A. Raman Spectroscopy Study of Rotated Double-Layer Graphene: Misorientation-Angle Dependence of Electronic Structure. *Phys. Rev. Lett.* 2012, 108, 246103.
 47. Neto, A. H. C.; Novoselov, K. New Directions in Science and Technology: Two-Dimensional Crystals. *Rep. Prog. Phys.* 2011, 74, 082501.
 48. Ferralis, N. Probing Mechanical Properties of Graphene with Raman Spectroscopy. *J. Mater. Sci.* 2010, 45, 5135-5149.
 49. Bae, S.; Kim, H.; Lee, Y.; Xu, X. F.; Park, J. S.; Zheng, Y.; Balakrishnan, J.; Lei, T.; Kim, H. R.; Song, Y. I.; *et al.* Roll-to-Roll Production of 30-Inch Graphene Films for Transparent Electrodes. *Nat. Nanotechnol.* 2010, 5, 574-578.

50. Koh, Y. K.; Bae, M. H.; Cahill, D. G.; Pop, E. Reliably Counting Atomic Planes of Few-Layer Graphene ($N > 4$). *ACS Nano* 2011, 5, 269-274.
51. Gorbachev, R. V.; Riaz, I.; Nair, R. R.; Jalil, R.; Britnell, L.; Belle, B. D.; Hill, E. W.; Novoselov, K. S.; Watanabe, K.; Taniguchi, T.; *et al.* Hunting for Monolayer Boron Nitride: Optical and Raman Signatures. *Small* 2011, 7, 465-468.
52. Das, A.; Chakraborty, B.; Piscanec, S.; Pisana, S.; Sood, A. K.; Ferrari, A. C. Phonon Renormalization in Doped Bilayer Graphene. *Phys. Rev. B* 2009, 79, 155417.
53. Das, A.; Pisana, S.; Chakraborty, B.; Piscanec, S.; Saha, S. K.; Waghmare, U. V.; Novoselov, K. S.; Krishnamurthy, H. R.; Geim, A. K.; Ferrari, A. C.; *et al.* Monitoring Dopants by Raman Scattering in an Electrochemically Top-Gated Graphene Transistor. *Nat. Nanotechnol.* 2008, 3, 210-215.
54. Yu, V.; Whiteway, E.; Maassen, J.; Hilke, M. Raman Spectroscopy of the Internal Strain of a Graphene Layer Grown on Copper Tuned by Chemical Vapor Deposition. *Phys. Rev. B* 2011, 84, 205407.
55. He, R.; Zhao, L. Y.; Petrone, N.; Kim, K. S.; Roth, M.; Hone, J.; Kim, P.; Pasupathy, A.; Pinczuk, A. Large Physisorption Strain in Chemical Vapor Deposition of Graphene on Copper Substrates. *Nano Lett.* 2012, 12, 2408-2413.
56. Lee, D. S.; Riedl, C.; Krauss, B.; von Klitzing, K.; Starke, U.; Smet, J. H. Raman Spectra of Epitaxial Graphene on Sic and of Epitaxial Graphene Transferred to SiO₂. *Nano Lett.* 2008, 8, 4320-4325.
57. Cullen, W. G.; Yamamoto, M.; Burson, K. M.; Chen, J. H.; Jang, C.; Li, L.; Fuhrer, M. S.; Williams, E. D. High-Fidelity Conformation of Graphene to SiO₂ Topographic Features. *Phys. Rev. Lett.* 2010, 105, 215504.
58. Yates, B.; Overy, M. J.; Pirgon, O. Anisotropic Thermal-Expansion of Boron-Nitride .1. Experimental Results and Their Analysis. *Philos. Mag.* 1975, 32, 847-857.
59. Zhuravlev, L. T. The Surface Chemistry of Amorphous Silica. Zhuravlev Model. *Colloid Surf. A-Physicochem. Eng. Asp.* 2000, 173, 1-38.
60. Zacharia, R.; Ulbricht, H.; Hertel, T. Interlayer Cohesive Energy of Graphite from Thermal Desorption of Polyaromatic Hydrocarbons. *Phys. Rev. B* 2004, 69, 155406.
61. Koenig, S. P.; Boddeti, N. G.; Dunn, M. L.; Bunch, J. S. Ultrastrong Adhesion of Graphene Membranes. *Nat. Nanotechnol.* 2011, 6, 543-546.
62. Casiraghi, C.; Pisana, S.; Novoselov, K. S.; Geim, A. K.; Ferrari, A. C. Raman Fingerprint of Charged Impurities in Graphene. *Appl. Phys. Lett.* 2007, 91, 233108/1-233108/3.
63. Geringer, V.; Liebmann, M.; Echtermeyer, T.; Runte, S.; Schmidt, M.; Ru"ckamp, R.; Lemme, M. C.; Morgenstern, M. Intrinsic and Extrinsic Corrugation of Monolayer Graphene Deposited on SiO₂. *Phys. Rev. Lett.* 2008, 102, 076102.
64. Mashoff, T.; Pratzer, M.; Geringer, V.; Echtermeyer, T. J.; Lemme, M. C.; Liebmann, M.; Morgenstern, M. Bistability and Oscillatory Motion of Natural Nanomembranes Appearing within Monolayer Graphene on Silicon Dioxide. *Nano Lett.* 2010, 10, 461-465.
65. Berciaud, S.; Ryu, S.; Brus, L. E.; Heinz, T. F. Probing the Intrinsic Properties of Exfoliated Graphene: Raman Spectroscopy of Free-Standing Monolayers. *Nano Lett.* 2009, 9, 346-352.
66. Lee, C.; Yan, H.; Brus, L. E.; Heinz, T. F.; Hone, J.; Ryu, S. Anomalous Lattice Vibrations of Single- and Few-Layer MoS₂. *ACS Nano* 2010, 4, 2695-2700.
67. Bukowska, H.; Meinerzhagen, F.; Akcoltekin, S.; Ochedowski, O.; Neubert, M.; Buck, V.; Schleberger, M. Raman Spectra of Graphene Exfoliated on Insulating Crystalline Substrates. *New J. Phys.* 2011, 13, 063018.
68. Ni, Z. H.; Wang, H. M.; Ma, Y.; Kasim, J.; Wu, Y. H.; Shen, Z. X. Tunable Stress and Controlled Thickness Modification in Graphene by Annealing. *ACS Nano* 2008, 2, 1033.

69. Bao, W.; Miao, F.; Chen, Z.; Zhang, H.; Jang, W.; Dames, C.; Lau, C. N. Controlled Ripple Texturing of Suspended Graphene and Ultrathin Graphite Membranes. *Nat. Nanotechnol.* 2009, 4, 562-566.
70. Malard, L. M.; Moreira, R. L.; Elias, D. C.; Plentz, F.; Alves, E. S.; Pimenta, M. A. Thermal Enhancement of Chemical Doping in Graphene: A Raman Spectroscopy Study. *J. Phys.-Condes. Matter* 2010, 22, 334202.
71. Abdula, D.; Ozel, T.; Kang, K.; Cahill, D. G.; Shim, M. Environment-Induced Effects on the Temperature Dependence of Raman Spectra of Single-Layer Graphene. *J. Phys. Chem. C* 2008, 112, 20131-20134.
72. Liu, H. T.; Liu, Y. Q.; Zhu, D. B. Chemical Doping of Graphene. *J. Mater. Chem.* 2011, 21, 3335-3345.
73. Ferralis, N.; Maboudian, R.; Carraro, C. Evidence of Structural Strain in Epitaxial Graphene Layers on 6h-Sic(0001). *Phys. Rev. Lett.* 2008, 101, 156801.
74. Rohrl, J.; Hundhausen, M.; Emtsev, K. V.; Seyller, T.; Graupner, R.; Ley, L. Raman Spectra of Epitaxial Graphene on Sic(0001). *Appl. Phys. Lett.* 2008, 92, 201918
75. Ni, Z. H.; Chen, W.; Fan, X. F.; Kuo, J. L.; Yu, T.; Wee, A. T. S.; Shen, Z. X. Raman Spectroscopy of Epitaxial Graphene on a Sic Substrate. *Phys. Rev. B* 2008, 77, 115416.
76. Sutter, P. W.; Flege, J.-I.; Sutter, E. A. Epitaxial Graphene on Ruthenium. *Nat. Mater.* 2008, 7, 406-411.

Figure legends

Figure 1. Morphology of graphene-hBN heterostack. (a) Optical micrograph of hBN/SiO₂/Si covered with CVD-grown graphene (sample **G1**), where 1L_{BN} and 1L_{SiO₂} designate graphene areas contacting hBN and SiO₂, respectively. (b) Non-contact AFM height image (9x9 μm²) obtained from the area within the yellow square in (a). (c) Non-contact AFM height image (2x2 μm²) obtained from the area within the white square in (b). (d) Height profile averaged from the yellow rectangle in (c). The thickness of the hBN flake, defined by the height difference between the two shaded regions in (d), is 3.4 ± 0.2 nm. (e) Height histograms of bare hBN (red circles) and SiO₂ substrates (blue circles). Roughness defined by standard deviation for Gaussian distribution in solid curves was 90 and 280 pm, respectively. The blue square in (a) marks the area where the Raman maps shown in Fig. 2 were obtained. The yellow arrows in (a) & (b) indicate areas where graphene was ruptured and folded during the transfer process.

Figure 2. Raman spectra and maps of graphene-hBN heterostack. (a) Raman spectra of 1L_{BN} and 1L_{SiO₂} (**G1**). D, G and 2D denote Raman peaks, respectively, originating from D mode, G mode and overtone of D mode. The peak denoted BN is due to E_{2g} phonon mode of hBN crystal. The detailed spectra (black squares for 1L_{SiO₂} and red circles for 1L_{BN}) separately shown for the D peak region reveal the presence of BN peak along with D peak for 1L_{BN}, with both peaks well described by double Lorentzian functions (orange and green lines). (b) Raman map for BN peak area (A_{BN}). (c) Raman map for G peak frequency

(ω_G). (d) Raman map for 2D peak frequency (ω_{2D}). (e) Raman map for G peak linewidth (Γ_G). (f) Raman map for 2D-to-G peak area ratio (A_{2D}/A_G). Mapping was carried out by raster scanning the blue squared region ($20 \times 20 \mu\text{m}^2$) in Fig. 1(a) with each pixel corresponding to an area of $1 \times 1 \mu\text{m}^2$. The dotted black lines in (b) ~ (f) represent the boundary of the hBN flake shown in Fig. 1(a).

Figure 3. Raman spectral analysis of graphene-BN heterostack. (a) Correlation between ω_G and ω_{2D} of **G1** (red symbols) and **G2** (blue symbols). Crosses and open circles represent $1L_{\text{BN}}$ and $1L_{\text{SiO}_2}$, respectively. Brown squares and triangles, obtained respectively from pristine and thermally annealed graphene/SiO₂ (Ref. 38), are shown for comparison. Inset: The arrows labeled e_T , e_C , e_H and e_{FVR} represent the trajectories of $\mathbf{O}(\omega_G, \omega_{2D})$ affected respectively by tensile strain, compressive strain, hole doping and vdW interlayer interaction leading to Fermi velocity reduction. The tick labels for ε on the e_T axis in (a) are given assuming uniaxial strain (Ref. 36) and those for n and $\Delta v_F/v_F$ along e_H and e_{FVR} are based on Ref. 52 and Ref. 43, respectively. (b) A_{2D}/A_G of **G1** and **G2** as a function of ω_G . The green dot and solid line represent average A_{2D}/A_G of freestanding graphene (Ref. 38) with uncertainty marked by the error bars and dotted lines. The black circles and error bars represent respectively average and standard deviation values for $1L_{\text{SiO}_2}$ data, whereas orange squares and error bars correspond to those for $1L_{\text{BN}}$ data.

Figure 4. The effects of thermal annealing on strain and charge doping. (a) Correlation between ω_G and ω_{2D} of **G3** obtained before (blue symbols) and after (red symbols) thermal annealing for 2 hours at 400 °C in vacuum. Crosses and open circles represent $1L_{\text{BN}}$ and $1L_{\text{SiO}_2}$, respectively. (b) A_{2D}/A_G of **G3** as a function of ω_G . The green dot and solid line represent average A_{2D}/A_G of freestanding graphene (Ref. 38) with uncertainty marked by the error bars and dotted lines. The black circles and error bars represent respectively average and standard deviation values for $1L_{\text{SiO}_2}$ data, whereas orange squares and error bars correspond to those for $1L_{\text{BN}}$ data.

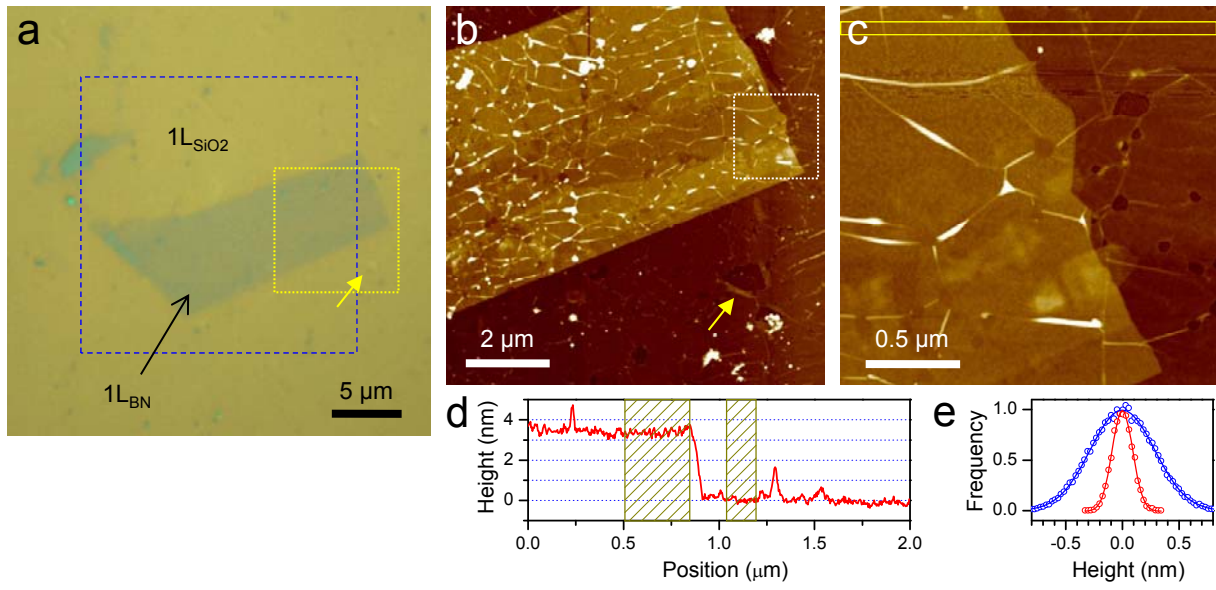


Figure 1. G. Ahn et al.

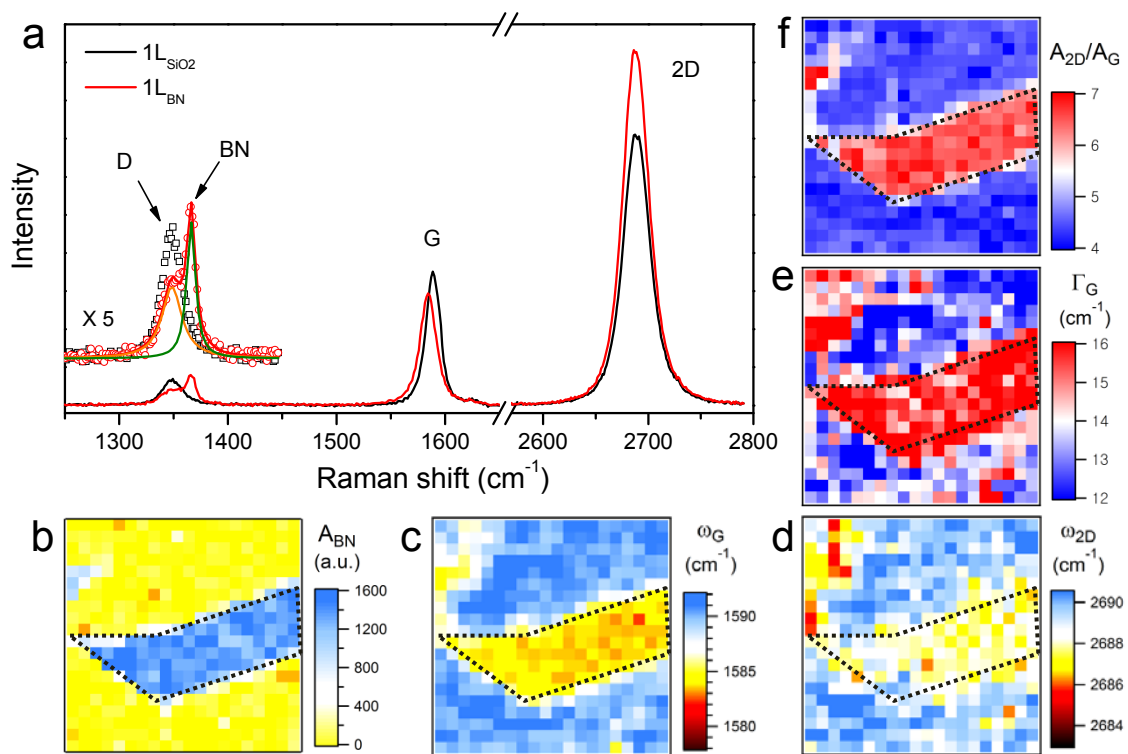


Figure 2. G. Ahn et al.

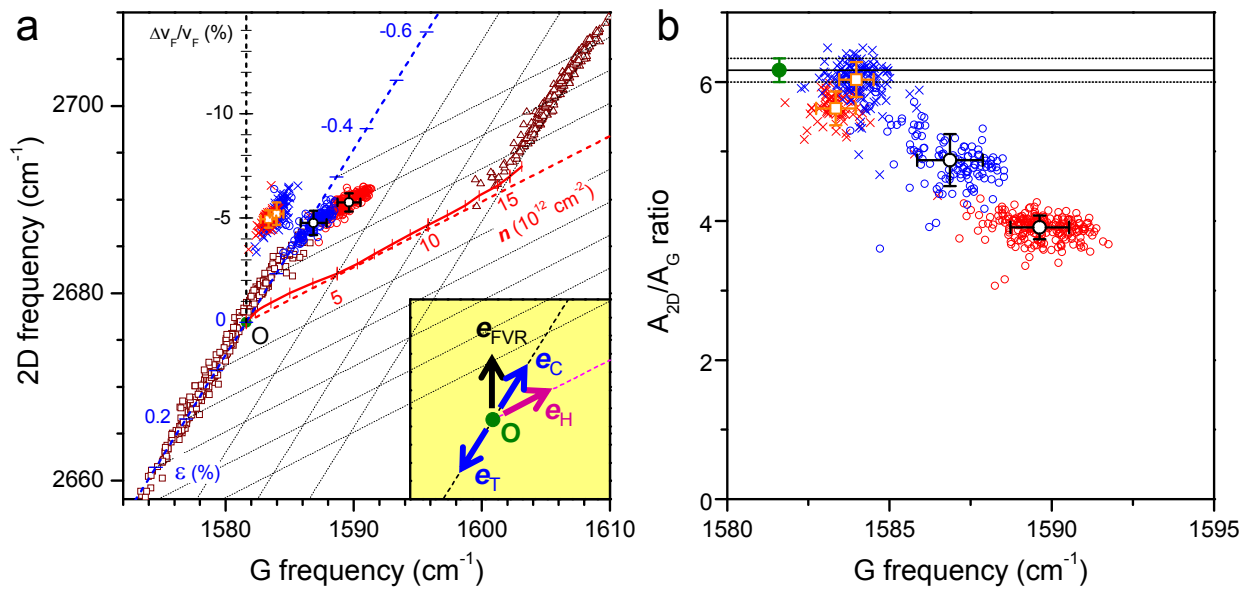


Figure 3. G. Ahn et al.

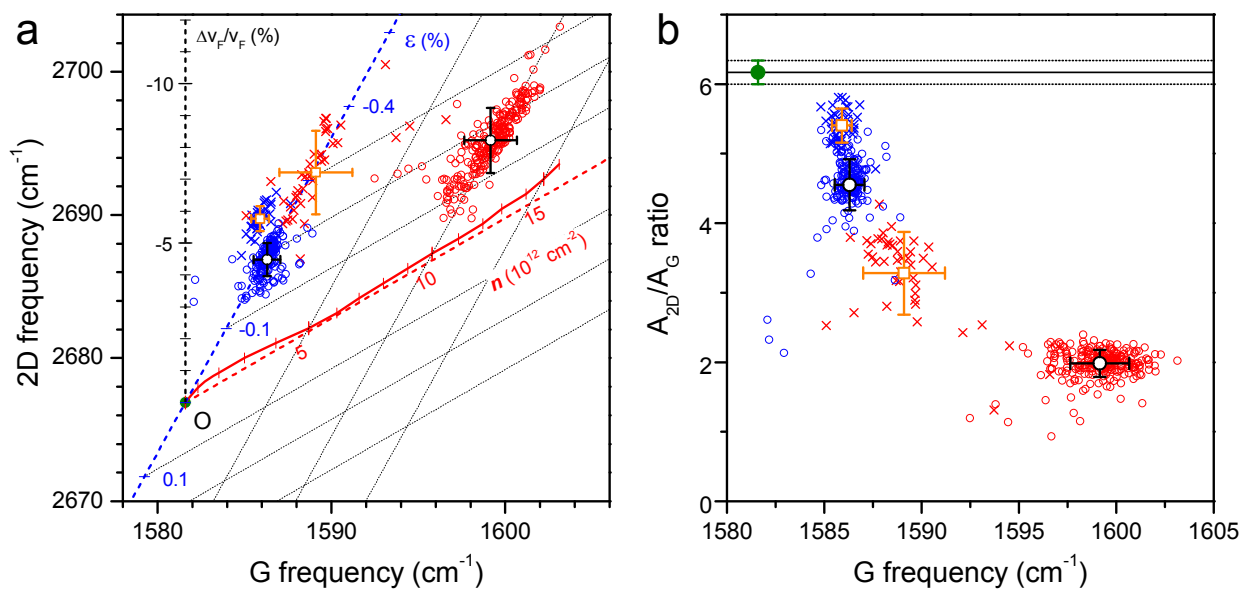


Figure 4. G. Ahn et al.